Application of Landsat-derived vegetation trends over South Africa: Potential for monitoring land degradation and restoration

Zander Samuel Venter[1,2], Samantha Luise Scott[3], Philip G Desmet[4] and Michael Timm Hoffman[3]

[1] Terrestrial Ecology Section, Norwegian Institute for Nature Research - NINA, 0349 Oslo, Norway

[2] ZSV Consulting, Unit 104, Sunstone, Ruby Estate, Marquise Drive, Burgundy Estate, South Africa

[3] Plant Conservation Unit, Department of Biological Sciences, University of Cape Town, Private Bag X3, Rondebosch 7701, South Africa

[4] Nelson Mandela University, Department of Zoology, PO Box 77000, Port Elizabeth, 6031, South Africa

Abstract

Monitoring vegetation change is important because the nature, extent and rate of change in key measures, such as plant biomass, cover and species composition, provides critical insight into broader environmental and land use drivers and leads to the development of appropriate policy. We used Landsat data between 1984 and 2018 to produce a map of Enhanced Vegetation Index (EVI) change over South Africa at 30 m resolution and an interactive web application to make the analysis both globally applicable and locally meaningful. We found an increase in EVI of 0.37 ± 0.59% yr^{-1} (mean ± standard deviation), confirming global vegetation greening trends observed with lower-resolution satellites. Mesic, productive biomes including the Albany Thicket and Savanna, exhibited the largest greening trends while browning trends were dominant in more arid biomes, such as the Succulent Karoo and Desert. Although overall EVI trends correspond to vegetation index trends derived from the Advanced Very-High-Resolution Radiometer (8 km resolution), the relative scarcity of Landsat data availability during the 1980s is a potential source of error. Using repeat very-high-resolution satellite (ca. 3 m resolution) imagery and ground-based photography as reference, we found good correspondence with EVI trends, revealing patterns of degradation (e.g. woody plant encroachment, desertification), and restoration (e.g. increased rangeland productivity, alien clearing) over selected landscapes. The utility of the EVI trend layer to government and industry for monitoring ecosystem changes will be enhanced by the ability to distinguish climatic from anthropogenic drivers of change. This may be partially achieved though interactive exploration of the EVI trends using the application found here: http://evitrend.zsv.co.za

Key words: *bush encroachment; desertification; ecosystem accounts; net primary productivity; remote sensing; repeat photography*

Introduction

Land degradation can be defined as the reduction or loss of ecosystem function caused by both human and non-human processes (Aynekulu et al., 2017). Reduced ecosystem function results in the loss of biodiversity and ecosystem services that sustain livelihoods around the globe, and is estimated to reduce the world's gross domestic product by 10-17% annually (ELD, 2015). Human-induced land degradation results from activities, such as the over-exploitation of natural resources, where vegetation is the primary terrestrial resource (Haberl et al., 2007). This is often associated with a reduction of vegetation cover, loss of natural habitat, and pollution and waste. In some environments an increase in vegetation cover, associated with woody plant thickening (Belay et al., 2013), or the invasion of alien species (Witt et al., 2017), can also result in the loss of ecosystem functionality, although this is not universally the case (Eldridge et al., 2011). Degradation trends can also be a result of climatic variability and trends, particularly in rainfall and temperature, that are unrelated to human activity (Ellis and Swift, 1988). Regardless of the cause, the Sustainable Development Goals acknowledge the global impact of degradation and now include Land Degradation Neutrality (LDN) as an important target with the aim of reversing existing land degradation and avoiding future degradation (Cowie et al., 2018). Achieving LDN requires an account of current ecosystem state, the extent of change relative to a given baseline, and an understanding of the main drivers of degradation. While climate change can exacerbate land degradation (Gonzalez et al., 2012), distinguishing anthropogenic and climatic drivers of vegetation cover change remains difficult.

In drylands, which cover 41% of the Earth's terrestrial surface (Maestre et al., 2016), degradation has historically been synonymous with desertification (Bauer, 2016; Sinclair and Fryxell, 1985) and is often associated with the overgrazing of rangelands by pastoralists (Hilker et al., 2014; Mganga et al., 2015). This narrative, however, has long been challenged by tenants of the non-equilibrium theory (Behnke et al., 1994), which holds that, in most dryland environments, vegetation cover is not in equilibrium with human-enforced herbivore pressures (Ellis and Swift, 1988). Rather, climatic variation can override the effect of human-induced degradation, so that vegetation cover can be restored or further degraded during rainfall extremes regardless of herbivore pressures. Despite the important influence that climate has on vegetation cover and composition, recent evidence from southern Africa suggests that the broad-scale recovery of vegetation in some of the region's dryland environments is probably linked more strongly to a release from historically high grazing pressure than to any underlying change in rainfall (Hoffman et al., 2018). Regardless of the drivers of change, distinguishing between trajectories of recovery and degradation is important in order to prioritise areas in need of restoration intervention.

Measuring trends in vegetation cover change has been made easier and more affordable at regional scales with the advent of free satellite remote sensing data (Wulder et al., 2012). Various satellite-derived vegetation indices have been used to measure attributes of ecosystem status including grassland and rangeland productivity (e.g. Cawkwell et al., 2016; Svoray et al., 2013) and degradation (e.g. Wessels et al., 2007), forest intactness (e.g. Hansen et al., 2013), land cover change (e.g. Defries and Townshend, 1994) and even ecosystem biodiversity (e.g. Gould, 2000), to name a few. These vegetation indices mostly rely on reflectance in the near-infrared wavelengths because plants have a distinctive spectral signature, characterised by a low reflectance in the visible spectrum, and a high reflectance in the near-infrared (Gates, 2012). A wealth of studies have used low spatial, but high temporal resolution satellite sensors such as the Moderate Resolution Imaging Spectrometer (MODIS) and the Advanced Very-High-Resolution Radiometer (AVHRR) to perform time series analysis of vegetation indices including the Normalised Difference Vegetation Index (NDVI) and the Enhanced Vegetation Index (EVI) as proxies for vegetation cover and primary productivity (Pettorelli et al., 2005; Tucker, 1979; Verbesselt et al., 2010). A wide-spread vegetation greening trend has been observed globally, which has been attributed to atmospheric CO_2 enrichment and increasing rainfall (Hickler et al., 2005; Zhu et al., 2016). Isolating local-scale drivers of change is made difficult by the low spatial resolution of MODIS (250 m) and AVHRR (8 km) imagery. In the context of LDN, useful tools, including Trends.Earth, have been developed to implement systematic accounts of land degradation using MODIS primary productivity trajectories (Gonzalez-Roglich et al., 2019). However, MODIS only extends back to 2000, and human-induced degradation footprints can occur at scales smaller than the 250 m MODIS resolution. Thus, higher resolution imagery might elucidate finer-scale dynamics.

Recent advances in cloud computing technology have allowed scientists to utilise the full archive of higher resolution (30 m) Landsat 5, 7 and 8 satellite imagery (extending back to 1984) to perform decadal time series analyses of vegetation cover change (Pasquarella et al., 2016). Remote sensing analysis has been able to move from static, bi-temporal measures of change toward more continuous time series analysis. Applications have included quantifying forest cover change (Hansen et al., 2013) and phenology (Melaas et al., 2013), land cover change (Gong et al., 2019), woody plant encroachment (Venter et al., 2018), riparian zone restoration (Hausner et al., 2018), and surface coal mining (Yang et al., 2018). Such studies provide a distinct advantage over low resolution regional measures of greening and browning trends because they give more nuanced insight into the type and cause of vegetation degradation or restoration.

This is particularly important in southern Africa where vegetation greening can signal both restoration and degradation, depending on the local context. For example, the encroachment of woody plants (alien or native) into open areas and an increase in grass cover can both be registered as greening by

satellites. However, woody plant encroachment often reduces the grazing capacity of a rangeland, while an increase in grass cover has the opposite effect (Anadón et al., 2014; Macharia and Ekaya, 2005). Previous efforts at identifying degradation using satellite remote sensing have focussed on distinguishing climate- versus human-driven browning (Wessels et al., 2007). Such efforts have either relied on expert opinion mapping at administrative unit scales, or have relied on the interpretation of single-temporal NDVI snapshots (Thompson et al., 2009). High-resolution land cover change maps do exist (e.g. GeoTerraImage, 2015) but they rely on a bi-temporal and categorical analysis of change only, that masks gradual changes along a continuum of vegetation cover. Government investment in alien clearing, wetland restoration, land development monitoring, rangeland management, and ecosystem accounts would benefit from monitoring tools that quantify trends in vegetation condition at high-resolution in an interactive environment that also allows for its integration with local knowledge. Furthermore, the Intergovernmental Science-Policy Platform on Biodiversity and Ecosystem Services (IPBES, 2018) has recognized the global importance of improving the detection, monitoring and verification of land degradation trends.

To improve upon previous analyses of vegetation cover change over South Africa at low spatial resolutions, we aimed to develop a high-resolution map of vegetation cover change and perform a quantitative and qualitative validation using ancillary satellite and fixed-point repeat photograph data at select locations over the country. We mapped linear trends in annual Landsat EVI time series for South Africa between 1984 and 2018 and hypothesised that the country has undergone a net greening in accordance with previous national-scale studies (Bai & Dent 2007). To make the layer relevant to policy makers and land managers, we have packaged it in an interactive web application that allows users with local knowledge to interpret vegetation dynamics at the landscape-scale. We illustrate this interpretation using very high-resolution satellite imagery and fixed-point repeat photographs for select locations across the country.

Methods

Remote sensing

All remote sensing data collection and analysis was performed using the Google Earth Engine (GEE) JavaScript API, which is a cloud computing platform for earth observation and analysis (Gorelick et al., 2017). We used the near-complete set of USGS Landsat 5, 7 and 8 Surface Reflectance Tier 1 imagery over South Africa at 30 m resolution between 1984 and 2019 (Woodcock et al., 2008). The Landsat data provided by GEE have been pre-processed to orthorectified surface reflectance and have been

atmospherically corrected using LEDAPS (Masek et al., 2006). We masked clouds, cloud shadow and snow using the 'pixel_qa' band. Due to slight differences between Landsat 7 and 8 sensors (Holden and Woodcock, 2016), cross-calibration of reflectance values is important when implementing time series analysis (Zhu, 2017). We applied published cross-calibration coefficients to harmonise Landsat 8 reflectance values with the other Landsat collections (Roy et al., 2016).

The most widely used satellite-derived measure of vegetation growth or vigour is (NDVI devised by Tucker (1979). However, NDVI saturates over high biomass areas and is sensitive to background soil reflectance and atmospheric contamination (Xue and Su, 2017). Despite the disadvantage of being less sensitive to sparse vegetation (Heute et al., 2012), EVI simultaneously corrects for atmospheric and soil effects and does not saturate over high vegetation biomass (Liu and Huete, 1995). Therefore we decided to use EVI even though EVI and NDVI are highly correlated over space and time (Fensholt et al., 2006). EVI is calculated as:

$$EVI = G \times \frac{\rho_{nir} - \rho_{red}}{\rho_{nir} + (C_1 \times \rho_{red} - C_2 \times \rho_{blue}) + L}$$

where ρ_{nir}, ρ_{red}, and ρ_{blue} represent reflectance in the near-infrared, red and blue wavelengths, and G=2.5, C_1=6, C_2=7.5, and L=1 (Huete et al., 2002).

Trend analysis

We derived time-integrated measures of EVI using medoid composites of reflectance values within each year. The medoid is a multi-dimensional analogue of the median which is robust against extreme outliers (e.g. remnant cloudy pixels after cloud masking) and is a better representative of vegetation conditions over the given time period compared to the more commonly used compositing methods such as median or maximum (Flood, 2013). The magnitude and significance of the trend in EVI between 1986 and 2019 was then calculated using the Sen's slope (Sen, 1968) estimator and Mann-Kendall test (Mann, 1945), respectively. The Sen's slope estimator is a non-parametric linear regression that is robust against outliers and skewed data (Wilcox, 2010). We calculated per-pixel percentage change in EVI as:

$$\Delta\, EVI = \frac{m}{c} \times 100$$

where m and c are the slope and y-intercept in the regression line defined as $y = mx + c$. Change in EVI is thus expressed relative to the baseline EVI value (y-intercept) for each pixel so that the magnitude of change is comparable across productivity gradients. Although the Sen's slope deals well with outliers, trends with large magnitudes are not necessarily significant because of large variance over time. Thus, the significance of the trend was calculated using the Mann-Kendall S statistic, which is

the most common non-parametric method to detect monotonic trends in climatic (e.g. Ahmad et al., 2015) and remote sensing (e.g. de Jong et al., 2011) data. To avoid the pitfalls of setting absolute significance levels (Amrhein et al., 2019), we used the S statistic as a weighting variable to calculate weighted means of EVI trends for spatial aggregations. We did this by scaling the S statistic scores over the country between 0 and 1, and multiplying each pixel's trend value by its scaled S statistic.

Mean EVI trend values were calculated for South African biomes and South Africa Vegetation Types (Mucina et al., 2018) grouped into ecological functional groups (Dayaram et al., 2019). South African Vegetation Types are mapped in terms of their historic or pre-European extent, i.e. natural vegetation extent prior to conversion to other land uses. We used a Landsat-derived 2014 land cover map (GeoTerraImage, 1990) to mask out water and non-natural (mine/industrial, plantation, cropland, built up) land cover categories when calculating mean EVI trends. Areas classified as "desert" in the land cover map were not masked because they were found to contain sparse vegetation elements that are of relevance to rangeland and conservation management.

Remote sensing validation

Validating our remote sensing product is made difficult by the fact that there are currently no published maps of decadal-scale ecosystem degradation or vegetation cover trends in South Africa (Driver et al., 2012). Thus, we utilised three reference datasets, namely (1) long-term, low resolution satellite measures of NDVI, (2) very high-resolution satellite red-green-blue (RGB) imagery and (3) fixed-point repeat photography for select locations over the country.

NDVI data from AVHRR sensors (in operation since 1981) have been widely used to quantify broad-scale trends in vegetation cover over the globe at a spatial resolution of 8 km (e.g. Cook and Pau, 2013; Fensholt et al., 2009; Gichenje and Godinho, 2018). Unlike the Landsat archive, the AVHRR data have a high temporal frequency and produce annual composites that are less affected by outliers introduced by cloud cover. Landsat data since 1984 have been collected by three different sensors and, without cross-sensor calibration, produce artificial anomalies in reflectance time series (Roy et al., 2016). Although the AVHRR sensors lack reliable calibration devices (Staylor, 1990; Burrell et al., 2018), and have relatively broad spectral bands, which reduce atmospheric correction accuracies (Tanre et al., 1992), they do provide a useful reference dataset for Landsat-derived vegetation indices (Beck et al., 2011). We calculated annual medoid mosaics for the Global Inventory Modeling and Mapping Studies (GIMMS; Tucker et al., 2005) third generation AVHRR NDVI dataset provided by GEE at a spatial resolution of 5 arc minutes between 1984 and 2013 (the AVHRR sensor was discontinued in 2013). The annual Landsat EVI medoids were aggregated to the spatial resolution of GIMMS data

using a mean reducer for comparison with GIMMS using a linear regression of all pixel values over South Africa for each year.

We performed a further qualitative validation and interpretation of landscape-scale trends using repeat satellite imagery and fixed-point repeat photographs. This validation was neither comprehensive nor quantitative because of the limited availability of metadata associated with validation photos which precluded quantitative estimates of vegetation cover change. They merely provide an analytical tool with which to illustrate what a range of browning and greening trends look like at landscape scales. Very high-resolution (<5 m) RGB satellite imagery from DigitalGlobe was filtered for 2002/4 and 2019 imagery using Google Earth Pro. Based on expert knowledge of known vegetation cover trends over the country, we manually located 14 landscapes expected to cover a variety of EVI trends (Fig. 1A). We manually selected Landsat pixel locations for comparison with visually-interpreted trends visible in DigitalGlobe images. Repeat fixed-point photographs, archived at the Plant Conservation Unit at the University of Cape Town (see http://rephotosa.adu.org.za), were filtered for photo pairs in which the repeat photograph was taken after 2010 so as to overlap with the Landsat data (1984-2018). Some historical photographs were taken decades before 1984 and thus comparisons with the Landsat EVI trends assume linear trends in vegetation cover reflected in repeat photographs. For qualitative analysis and interpretation, we selected 8 historical-repeat photo pairs showing a range of vegetation cover trends over different vegetation types. Photo locations (Fig. 1A) reported by photographers using a GPS were visualised in Google Earth Pro using the 3D view mode to digitise the photograph field-of-view over the landscape for comparison with the Landsat EVI trend raster image. One or two pixels were selected over the landscape for EVI trend inspection.

Results

Overall trends

South Africa has undergone a net greening between 1984 and 2018 with a mean EVI trend of 0.67 ± 0.77% yr^{-1} (mean ± standard deviation) when quantifying change relative to the baseline EVI value for each pixel (Fig. 1). After weighting trend values by the Mann-Kendall statistic to account for trend significance, the mean value was 0.37 ± 0.59% yr^{-1} which equates to 12.6 ± 20% increase over the 34 years. The mean absolute change in EVI values over the country revealed an increase of 0.02 ± 0.046 EVI units yr^{-1}. Large greening trends dominate the central and northern parts of the country while browning trends are evident in parts of the east and over much of the extreme north western part of the country (Fig. 1A). The change in EVI was not evenly distributed across the long-term mean EVI

gradient (Fig. 1B) nor the South African biomes (Fig. 1C) or functional vegetation types (Fig. S2). Browning trends were largely restricted to areas with low average EVI (< 0.07), characteristic of the arid and semi-arid areas of the Succulent Karoo and Desert biomes and parts of the Nama-Karoo biome. Greening trends were highest in environments with long-term mean EVI values of ca. 0.2, particularly the Albany Thicket and Indian Ocean Coastal Belt biomes. Greening trends were relatively consistent in more productive, mesic areas, notably the Savanna biome which covers 32% of the country (Fig. 1C).

GIMMS validation

The mean Landsat EVI and GIMMS NDVI values are strongly correlated over South Africa (Fig. 2A). Annual deviations from long-term means for each pixel display positive trends for both Landsat and GIMMS sensors (Fig. 2B). However, Landsat data exhibit large positive biases compared to the GIMMS data during 1985, 1987 and again in 2009 and 2010 (Fig. 2B). This is likely due to the low number of available cloud-free pixels during those years, particularly during the 1980s. This introduces variation in the day-of-year at which the annual medoid value for each pixel was acquired (Fig. S2B). This may also explain the variance in trend values depending on the start and end date of EVI time series (Fig. S3).

Landscape-level validation

We present EVI greening and browning trends over selected landscapes to illustrate different change scenarios outlined in Table 1. Readers can explore trends at this resolution for different localities around the world interactively here: http://evitrend.zsv.co.za. Gradual greening trends may be associated with woody plant encroachment into previously grassy areas (Fig. 3A, Table 1), or an increase in the cover of woody plants on previously bare areas, such as eroded gullies in agricultural landscapes (Fig. 3B). Bush encroachment into grassy areas may be associated with a reduction in EVI seasonality over time (e.g. Fig. S9 & S10) due to the perennial phenology of woody vegetation greenness. Greening trends can also be indicative of an increase in herbaceous vegetation cover or vigour while woody plant cover has remained constant (Fig. 3C & D). Here, there is an increase in EVI seasonality due to the senescent phenology of many grass species.

Significant browning trends over areas previously covered by woody plants may indicate tree harvesting or clearing (Fig. 4D)and in some cases, the expansion of settlements in response to population growth (Fig. 4A). In areas dominated by herbaceous vegetation, browning may be indicative of overgrazing, which can result in a reduction in grass vigour and basal cover (Fig. 4A). In arid landscapes, where vegetation cover is generally low, browning trends might indicate a loss in

vegetation vigour (Fig. 4C). However, the relative change in arid areas should be viewed in terms of the magnitude of absolute changes, which may be very low (e.g. 0.01 EVI units in Fig. 4C). Browning trends are, therefore, not necessarily an indication of management-induced degradation but when viewed in context of rainfall trends, may be a product of long- or short-term drought conditions. The clearing of alien vegetation is an example of where restoration activity might exhibit a browning trend in the vegetation EVI (Fig. 4D). Abrupt browning, typically caused by fire (e.g. Fig. 4D), land cover change, or deforestation (see supplement for illustrations), are smoothed by the long-term EVI trend layer.

Discussion

Recent advances in computing power and the availability of large data have expanded the utility of satellite remote sensing in providing repeatable and standardised monitoring of long-term environmental trends (Pettorelli et al., 2014; Zhu, 2017). Despite this, there have been few national level analyses of how remotely-sensed indices of net primary productivity (NPP) have changed over time in South Africa. Using Landsat data, available from the Google Earth Engine platform, our results show an overall net increase in the enhanced vegetation index (EVI) of about 0.37 ± 0.59 % yr^{-1} over South Africa for the period 1984-2018. The general increasing trend corresponds to evidence at the global-scale for a net greening during the past three decades (Zhu et al., 2016). Increasing trends were greatest in the more humid eastern parts of the country where long-term, mean annual rainfall totals are above 200 mm. Negative trends were apparent in the arid and hyper-arid western parts of the country. This adds a different perspective on change, in both its temporal and spatial pattern, from earlier national-level assessments that were conducted over different time spans. For example, using NDVI values from fortnightly images at 8 km spatial resolution derived from the AVHRR sensor and produced by the Global Inventory Modelling and Mapping Studies (GIMMS) group, Bai and Dent (2007) suggested that for the period 1981-2003, net primary productivity had decreased over ca. 30% of South Africa. Their results also showed that the decrease was greatest in the humid and sub-humid eastern areas of South Africa and smallest in the more arid and hyper-arid, western parts of the country where NDVI values had generally increased over their study period. Although these findings cannot be directly compared to our results, the differences in spatio-temporal patterns of change underscore some of the difficulties in using remotely-sensed indices of NPP which can be strongly influenced by the start and end dates of the time series, the type of index used as well as by the spatial and temporal resolution of the data (Wessels et al., 2012).

While an analysis of the climatic and anthropogenic drivers of greening and browning trends was not within the scope of this study, we found that using fixed-point repeat photographs and high resolution satellite images as a form of qualitative validation gave insight into the attribution of degradation or restoration signals. This is particularly the case when interpreted relative to the local context of change. For example, much of the increase in EVI recorded in this study for the Albany Thicket, Indian Ocean Coastal Belt and Savanna biomes can probably be attributed to an increase in woody plant cover. Here, assigning the greening trend as degradation or restoration is complex given that woody plant encroachment can be detrimental for livestock agriculture, and yet beneficial for carbon sequestration (Foden et al., 2019). This encroachment or thickening of woody plants has been widely reported in these biomes (O'Connor et al., 2014; Skowno et al., 2017) although reasons for the increase differ. Widespread abandonment of cultivation (Shackleton et al., 2019), a change in burned area (Venter et al., 2018) or fire frequency (Singh et al., 2018), an increase in the concentration of CO_2 in the atmosphere (Bond and Midgley, 2000) and an increase in invasive alien plants (Nkambule et al. 2017) or even plantation forestry (Turpie et al. 2007) are all potential explanations for the pattern. In contrast, an increase in the cover of herbaceous grasses and not woody plants is probably responsible for the greening of the wide ecotone between the Nama-Karoo and Grassland biome in the central part of the country (Masubelele et al., 2015). For the Fynbos biome, the increase in EVI values within the Cape Fold Mountains as well as the more arid Kamiesberg and Roggeveld high-lying areas are more difficult to explain, especially in light of the severe drought that has occurred across much of the winter rainfall region over the period 2015-2017.

There has been a reduction in EVI recorded for the arid and hyper-arid north western parts of the winter rainfall region. Results from several repeat photography studies in the same region report an increase in the cover of perennial plants over landscape units composed of plains and ephemeral streams (Hoffman & Rohde, 2011) although these pre-date the more recent severe drought experienced in the winter rainfall region. Other areas which exhibited a browning trend in South Africa, such as parts of KwaZulu-Natal and the southern section of Kruger National Park, can be explained by factors other than climate. For example, Jewitt et al., (2015), showed that the expansion of agriculture, plantation forestry, settlements, dams and mines in KwaZulu-Natal were largely responsible for the transformation of 1.2% of the province's natural landscapes each year over the period 1994 to 2011. Therefore, the decrease in EVI values over parts of the province has likely occurred as a result of this increase in anthropogenic activities. A different explanation is likely for the browning trend recorded for Kruger National Park which is best understood in terms of the reported impact that megaherbivores have had on vegetation biomass in the park (Pellegrini et al., 2017).

To generate or map more generalized explanations for greening and browning trends over South Africa will require a more comprehensive validation approach. Due to the limited availability of ground-truth datasets, we resorted to a nuanced and qualitative validation using repeat fixed-point ground and satellite images. The repeat photograph epochs extend beyond the Landsat time frame (1984-2018) and therefore one has to assume linearity in trends that predate this. The use of GIMMS dataset was an attempt to supplement the qualitative approach and we found good correspondence with the Landsat EVI trends. Apart from merely validating the accuracy of EVI trends, making value judgements about the implications of greening or browning trends by assigning them to degradation or restoration categories requires more information on the drivers of change. For example, there are many methods to distinguish climatic from human-induced drivers of browning or greening using remote sensing data (e.g. Abel et al., 2019; Burrell et al., 2017; Horion et al., 2016; Wessels et al., 2007).

Remote sensing with both high- (e.g. Gonzalez et al., 2012) and low-resolution (e.g. Bai et al., 2008) satellite-derived indices of vegetation productivity can be used to monitor changes in the environment over relatively large spatial and temporal scales. However, these indices usually provide little more than a general screening tool and cannot adequately provide information on the type of degradation or improvement in a landscape. More detailed information on the nature of the changes observed and the reasons for the changes at smaller spatial and temporal scales can often only be inferred from extensive ground-truthing, from the observer's knowledge of the region, or from published studies of the area. Even then, it is difficult to include a temporal interpretation of the trajectories observed since very few locations have independent, long-term monitoring data sets to draw on. Data are also very seldom collected at time-scales relevant to those covered by satellite-derived data and mismatches between satellite spatial resolution and field data further complicate validation. In the approach presented here, however, two novel contributions are made.

Firstly, when used in combination with other remotely sensed measures, such as those resulting from repeat very-high-resolution satellite and ground photography, a more insightful and detailed interpretation of both the magnitude and direction of change, recorded by Landsat-derived EVI, is possible. We found good correspondence with EVI trends showing patterns of degradation (e.g. woody plant encroachment, desertification) and restoration (e.g. increased rangeland productivity, alien clearing) in South Africa. The inclusion of fine-scale measurement, such as is presented here, enables the observer to check on the broad-scale pattern provided by the satellite-derived vegetation index and, in some cases, to better understand local-level processes responsible for the change. The different spatial scales used in such an analysis also provide a more complete understanding of environmental change than is usually provided by analyses carried out at one spatial scale only.

A second contribution of this study relates to the accessibility and usability of satellite-derived vegetation indices. Cloud computing platforms such as Google Earth Engine (Gorelick et al., 2017) are making data collection, analysis and visualisation more accessible to scientists and non-specialists alike. The delivery of remote sensing products in web applications as opposed to static maps is becoming more common (e.g. Donchyts et al., 2016; Huntington et al., 2017). Users are allowed to interact with mapped data at their highest resolution, affording more locally-relevant insights than those gained from a printed map in a publication. The EVI trend data presented here can be explored at full resolution in our web application (http://evitrend.zsv.co.za). We intend for users to potentially decipher landscape-scale degradation and restoration trends based on local knowledge with the aid of plotted EVI trends for user-selected pixels over user-defined time periods (Fig. S3). With access to the EVI time series, users might be able to also identify periods of rapid change caused by fire or vegetation clearing events that are lost when summarising the time series using a linear regression line. In this manner, accuracy errors introduced by the low availability of Landsat data during the 1980s, and variation in trend values depending on start and end dates for EVI time series can be further interrogated. The biases in the day-of-year (Fig. S1B) during the 80s should inform user interpretation of trends depending on local vegetation phenology. For instance, the large bias toward Jan/Dec medoid EVI values in 1986-7 may introduce false-negative long-term trends in summer rainfall areas where EVI values are expected to be relatively high in Dec/Jan. Conversely, false-positive long-term trends might be more likely in winter rainfall areas.

Governments and industry partners within, but not limited to, South Africa would benefit from a cost-effective tool for measuring and monitoring ecosystem management and restoration interventions such as vegetation recovery after alien clearing or mine restoration, or the impact of de-stocking on rangeland vegetation cover. The EVI trend analysis presented here has wide application and relevance to a range of land users and decision making interested in incorporating information on the state and trend of ecosystems into land use management or economic enterprises. For example, livestock or wildlife managers might be able to assess seasonal patterns in vegetation productivity in the context of long-term trends in productivity at the grazing camp or farm-scale. Objective and repeatable measures of ecosystem extent and condition are essential for the successful implementation of ecosystem accounts (United Nations 2014, Driver *et al.* 2015). This EVI trend analysis is a step towards the development of an ecosystem condition index that meets these criteria and with a spatial resolution relevant to ecosystem accounting. By applying time series processing to intra-annual vegetation indices, real-time monitoring of land clearing is already being implemented using a fusion of Landsat and Sentinel satellite data to monitor tropical deforestation (Reiche et al., 2018). Translating such approaches to more arid environments should be possible with relevant ground-truth

data. Finally, by supplementing the EVI trend data with time series analyses aimed at disaggregating climatic from anthropogenic drivers (Burrell et al., 2017), it will be possible to understand their relative contribution to the observed trend. More importantly it will highlight where land use interventions are likely to have greater impacts on ecosystems and may contribute to global ecosystem accounting initiatives such as those outlined in the IPBES framework (Diaz et al., 2015).

Conclusion

While we observed an overall vegetation greening over South Africa between 1984 and 2018, we found the direction and magnitude of this trend to be spatially variable at regional and landscape scales. We suggest that while aggregating results at regional-scales is interesting, the ability to derive locally relevant insights is only realised at higher resolutions, as illustrated by validation and interpretation of the EVI trend layer with fixed-point repeat photography and very-high-resolution satellite imagery. The delivery of the EVI analysis and results in an interactive web application should allow users to gain local-scale insight at 30 m resolution, interrogate per-pixel EVI time series to identify sources of error, and to potentially integrate knowledge of local ecosystems to distinguish restoration from degradation signals in the EVI time series. The utility of the EVI trend layer to government and industry for monitoring ecosystem changes will be enhanced by the ability to distinguish climatic from anthropogenic drivers of change. This may be soon realised by fusing Landsat and Sentinel satellite data, allowing for high resolution monitoring in near real-time.

Acknowledgements

We are thankful to the two anonymous reviewers for their critical contribution to the improvement of the manuscript. Image credit for historical fixed-point photographs by Acocks, John Phillip Harison: © SANBI and licensed under Creative Commons licence CC-BY. More information can be found here: http://rephotosa.adu.org.za/

References:

Abel, C., Horion, S., Tagesson, T., Brandt, M., Fensholt, R., 2019. Towards improved remote sensing based monitoring of dryland ecosystem functioning using sequential linear regression slopes (SeRGS). Remote Sens. Environ. 224, 317–332. https://doi.org/https://doi.org/10.1016/j.rse.2019.02.010

Ahmad, I., Tang, D., Wang, T., Wang, M., Wagan, B., 2015. Precipitation trends over time using Mann-Kendall and spearman's rho tests in swat river basin, *Pakistan. Adv. Meteorol.* 2015. https://doi.org/10.1155/2015/431860

Amrhein, V., Greenland, S., McShane, B., 2019. Scientists rise up against statistical significance, *Nature*. 567, 305-307.

Anadón, J.D., Sala, O.E., Turner, B.L., Bennett, E.M., 2014. Effect of woody-plant encroachment on livestock production in North and South America. *Proc. Natl. Acad. Sci.* 111, 12948 LP-12953. https://doi.org/10.1073/pnas.1320585111

Aynekulu, E., Lohbeck, M., Nijbroek, R., Ordoñez, J.C., Turner, K.G., Vågen, T.-G., Winowiecki, L., 2017. Review of methodologies for land degradation neutrality baselines: Sub-national case studies from Costa Rica and Namibia. CIAT Publication No. 441. International Center for Tropical Agriculture (CIAT) and World Agroforestry Center (ICRAF), Nairobi, Kenya. 58 p.

Bai, Z., Dent D., 2007. Land degradation and improvement in South Africa 1: Identification by remote sensing, Wageningen: International Soil Reference and Information Centre (ISRIC), Report 2007/03.

Bai, Z. G., Dent, D. L., Olsson, L., Schaepman, M. E., 2008. Proxy global assessment of land degradation. *Soil Use Manage.* 24, 223-234. doi:10.1111/j.1475-2743.2008.00169.x

Bauer, S., 2016. The United Nations and the Fight against Desertification: What Role for the UNCCD Secretariat?, in: Governing Global Desertification. Routledge, pp. 93–108.

Beck, H.E., McVicar, T.R., van Dijk, A.I.J.M., Schellekens, J., de Jeu, R.A.M., Bruijnzeel, L.A., 2011. Global evaluation of four AVHRR–NDVI data sets: Intercomparison and assessment against Landsat imagery. *Remote. Sens. Environ.* 115, 2547–2563. https://doi.org/10.1016/j.rse.2011.05.012

Behnke, R.H., Scoones, I., Kerven, C., 1994. Range Ecology at Disequilibrium, Range ecology at disequilibrium. Overseas Development Institute, London.

Belay, T. A, Totland, Ø., & Moe, S. R., 2013. Ecosystem responses to woody plant encroachment in a

448 semiarid savanna rangeland. *Plant Ecol. 214*, 1211-1222. doi: 10.1007/s11258-013-0245-3

449 Bond, W.J., Midgley, G.F., 2000. A proposed CO_2-controlled mechanism of woody plant invasion in
450 grasslands and savannas. *Glob. Chang. Biol*. 6, 865-869. DOI: 10.1046/j.1365-2486.2000.00365.x

451 Burrell, A.L., Evans, J.P., Liu, Y., 2017. Detecting dryland degradation using Time Series Segmentation
452 and Residual Trend analysis (TSS-RESTREND). Remote Sens. Environ. 197, 43–57.
453 https://doi.org/https://doi.org/10.1016/j.rse.2017.05.018

454 Burrell, A.L., Evans, J.P., Liu, Y., 2018. The impact of dataset selection on land degradation assessment.
455 ISPRS J. Photogramm. Remote Sens. 146, 22-
456 37. https://doi.org/10.1016/J.ISPRSJPRS.2018.08.017

457 Cawkwell, F., Ali, I., Green, S., Dwyer, E., Barrett, B., 2016. Satellite remote sensing of grasslands: from
458 observation to management. J. *Plant Ecol*. 9, 649–671. https://doi.org/10.1093/jpe/rtw005

459 Cook, I.B., Pau, S., 2013. A Global Assessment of Long-Term Greening and Browning Trends in Pasture
460 Lands Using the GIMMS LAI3g Dataset. *Remote Sens*. DOI: 10.3390/rs5052492

461 Cowie, A.L., Orr, B.J., Castillo Sanchez, V.M., Chasek, P., Crossman, N.D., Erlewein, A., Louwagie, G.,
462 Maron, M., Metternicht, G.I., Minelli, S., Tengberg, A.E., Walter, S., Welton, S., 2018. Land in
463 balance: The scientific conceptual framework for Land Degradation Neutrality. *Environ. Sci.*
464 *Policy*. 79, 25–35. DOI: https://doi.org/10.1016/j.envsci.2017.10.011

465 Dayaram, A., Desmet, P., Todd, S., Rebelo, T., Geldenhuys, C., Lotter, M., Hoare, D., Grobler, A.,
466 Slingsby, J., Moncrieff, G., Skowno, A., Forsythe, K. and Driver, A., 2019. Draft Working Version
467 of Proposed Functional Vegetation Groups for VEGMAP vegetation types 2018, Version 2. Cape
468 Town, South Africa.

469 de Jong, R., de Bruin, S., de Wit, A., Schaepman, M.E., Dent, D.L., 2011. Analysis of monotonic greening
470 and browning trends from global NDVI time-series. *Remote Sens. Environ.* 115, 692–702. DOI:
471 https://doi.org/10.1016/j.rse.2010.10.011

472 Defries, R.S., Townshend, J.R.G., 1994. NDVI-derived land cover classifications at a global scale. *Int. J.*
473 *Remote Sens*. 15, 3567–3586. DOI: https://doi.org/10.1080/01431169408954345

474 Díaz et al., 2015. The IPBES Conceptual Framework - connecting nature and people. Curr. Opin.
475 Environ. Sustain. 14, 1–16. https://doi.org/https://doi.org/10.1016/j.cosust.2014.11.002

476 Donchyts, G., Baart, F., Winsemius, H., Gorelick, N., Kwadijk, J., Van De Giesen, N., 2016. Earth's surface
477 water change over the past 30 years. *Nat. Clim. Chang. 6*, 810. DOI:

https://doi.org/10.1038/nclimate3111

Driver A., Sink, K.J., Nel, J.N., Holness, S., Van Niekerk, L., Daniels, F., Jonas, Z., Majiedt, P.A., Harris, L. & Maze, K., 2012. National Biodiversity Assessment 2011: An assessment of South Africa's biodiversity and ecosystems. Synthesis Report. South African National Biodiversity Institute and Department of Environmental Affairs, Pretoria.

Driver, D., Nel, J.L., Smith, J., Daniels, F., Poole, C.J., Jewitt, D., Escott, B.J., 2015. "Land and ecosystem accounting in KwaZulu-Natal, South Africa: Discussion document". Available at: http://biodiversityadvisor.sanbi.org/wp-content/uploads/2016/04/Land-and-Ecosystem-Accounting-in-KZN-Discussion-Document- FINAL.pdf.

ELD, 2015. Report for policy and decision makers: Reaping economic and environmental benefits from sustainable land management.

Eldridge, D. J., Bowker, M. A., Maestre, F. T., Roger, E., Reynolds, J. F. and Whitford, W. G., 2011. Impacts of shrub encroachment on ecosystem structure and functioning: towards a global synthesis. *Ecol. Lett.* 14: 709-722. doi: 10.1111/j.1461-0248.2011.01630.x

Ellis, J.E., Swift, D.M., 1988. Stability of African pastoral ecosystems: alternate paradigms and implications for development. Rangel. *Ecol. Manag. Range Manag. Arch.* 41, 450–459.

Fensholt, R., Sandholt, I., Stisen, S., 2006. Evaluating MODIS, MERIS, and VEGETATION vegetation indices using in situ measurements in a semiarid environment. IEEE Trans. Geosci. Remote Sens. 44, 1774-1786. https://doi.org/10.1109/TGRS.2006.875940

Fensholt, R., Rasmussen, K., Nielsen, T.T., Mbow, C., 2009. Evaluation of earth observation based long term vegetation trends — Intercomparing NDVI time series trend analysis consistency of Sahel from AVHRR GIMMS, Terra MODIS and SPOT VGT data. *Remote Sens. Environ.* 113, 1886–1898. DOI: https://doi.org/10.1016/j.rse.2009.04.004

Flood, N., 2013. Seasonal Composite Landsat TM/ETM+ Images Using the Medoid (a Multi-Dimensional Median). *Remote Sens.* 5(12), 6481-6500. DOI: https://doi.org/10.3390/rs5126481

Foden, W., Midgley, G., Kelly, C., Stevens, N. & Robinson, J.2019. 'Chapter 5: Pressures and Drivers III – Climate Change', in National Biodiversity Assessment 2018 Technical Report Volume 1: Terrestrial Realm. Skowno, A.L., Raimondo, D.C., Poole, C.J., Fizzotti, B. & Slingsby, J.A. (eds.). South African National Biodiversity Institute, Pretoria.

Gates, D.M., 2012. Biophysical ecology. Springer-Verlag, New York.

GeoTerraImage, 1990. Technical Report: 1990 South African National Land Cover Dataset version 5.2. Pretoria.

GeoTerraImage, 2015. DEA/CARDNO SCPF002: Implementation of Land- Use Maps for South Africa: 1990 - 2013/14 South African National Land-Cover Change Project Specific Data Report version 02. Report for the Department of Environmental Affairs, Pretoria. August 2015.

Gichenje, H., Godinho, S., 2018. Establishing a land degradation neutrality national baseline through trend analysis of GIMMS NDVI Time-series. *L. Degrad. Dev.* 29, 2985–2997. DOI: https://doi.org/10.1002/ldr.3067

Gong, P., Li, X., Zhang, W., 2019. 40-year (1978-2017) human settlement changes in China reflected by impervious surfaces from satellite remote sensing. *Sci. Bull.* 64(11), 756-763. DOI: https://doi.org/10.1016/j.scib.2019.04.024

Gonzalez, P., Tucker, C.J., Sy, H., 2012. Tree density and species decline in the African Sahel attributable to climate. *J. Arid Environ.* 78, 55–64. DOI: 10.1016/j.jaridenv.2011.11.001

Gonzalez-Roglich, M., Zvoleff, A., Noon, M., Liniger, H., Fleiner, R., Harari, N., Garcia, C., 2019. Synergizing global tools to monitor progress towards land degradation neutrality: Trends.Earth and the World Overview of Conservation Approaches and Technologies sustainable land management database. *Environ. Sci. Policy*. 93, 34–42. DOI: https://doi.org/10.1016/j.envsci.2018.12.019

Gorelick, N., Hancher, M., Dixon, M., Ilyushchenko, S., Thau, D., Moore, R., 2017. Google Earth Engine: Planetary-scale geospatial analysis for everyone. *Remote Sens. Environ.* 202, 18–27. DOI: https://doi.org/10.1016/j.rse.2017.06.031

Gould, W., 2000. Remote sensing of vegetation, plant species richness, and regional biodiversity hotspots. *Ecol. Appl.* 10, 1861–1870. DOI: 10.2307/2641244

Haberl, H., Erb, K.H., Krausmann, F., Gaube, V., Bondeau, A., Plutzar, C., Gingrich, S., Lucht, W., Fischer-Kowalski, M., 2007. Quantifying and mapping the human appropriation of net primary production in earth's terrestrial ecosystems. *Proc. Natl. Acad. Sci.* 104, 12942 LP-12947. DOI: https://doi.org/10.1073/pnas.0704243104

Hansen, M.C., Potapov, P. V, Moore, R., Hancher, M., Turubanova, S.A., Tyukavina, A., Thau, D., Stehman, S. V, Goetz, S.J., Loveland, T.R., 2013. High-resolution global maps of 21st-century forest cover change. *Science*. 342(6160), 850–853. DOI: 10.1126/science.1244693

Hausner, M.B., Huntington, J.L., Nash, C., Morton, C., McEvoy, D.J., Pilliod, D.S., Hegewisch, K.C.,

Daudert, B., Abatzoglou, J.T., Grant, G., 2018. Assessing the effectiveness of riparian restoration projects using Landsat and precipitation data from the cloud-computing application ClimateEngine.org. *Ecol. Eng.* 120, 432–440. DOI: https://doi.org/10.1016/j.ecoleng.2018.06.024

Hickler, T., Eklundh, L., Seaquist, J.W., Smith, B., Ardö, J., Olsson, L., Sykes, M.T., Sjöström, M., 2005. Precipitation controls Sahel greening trend. *Geophys. Res. Lett.* 32. https://doi.org/10.1029/2005GL024370

Hilker, T., Natsagdorj, E., Waring, R. H., Lyapustin, A. and Wang, Y., 2014. Satellite observed widespread decline in Mongolian grasslands largely due to overgrazing. *Glob. Chang. Biol*. 20: 418-428. doi:10.1111/gcb.12365

Hoffman, M.T., Rohde, R.F., 2011. Rivers through time: Historical changes in the riparian vegetation of the semi-arid, winter rainfall region of South Africa in response to climate and land use. J. Hist. Biol. 44, 59-80. DOI 10.1007/s10739-010-9246-4

Hoffman, M.T., Skowno, A., Bell, W., Mashele, S., 2018. Long-term changes in land use, land cover and vegetation in the Karoo drylands of South Africa: implications for degradation monitoring. *Afr. J. Range Forage Sci.* 35, 209–221. https://doi.org/10.2989/10220119.2018.1516237

Holden, C.E., Woodcock, C.E., 2016. An analysis of Landsat 7 and Landsat 8 underflight data and the implications for time series investigations. *Remote Sens. Environ.* 185, 16–36. DOI: https://doi.org/10.1016/j.rse.2016.02.052

Horion, S., Prishchepov, A. V, Verbesselt, J., de Beurs, K., Tagesson, T., Fensholt, R., 2016. Revealing turning points in ecosystem functioning over the Northern Eurasian agricultural frontier. Glob. Chang. Biol. 22, 2801–2817. https://doi.org/10.1111/gcb.13267

Huete, A., Didan, K., Miura, T., Rodriguez, E.P., Gao, X., Ferreira, L.G., 2002. Overview of the radiometric and biophysical performance of the MODIS vegetation indices. *Remote Sens. Environ.* 83, 195–213. DOI: https://doi.org/10.1016/S0034-4257(02)00096-2

Huntington, J. L., Hegewisch, K. C., Daudert, B., Morton, C. G., Abatzoglou, J. T., McEvoy, D. J., Erickson, T., 2017. Climate Engine: cloud computing and visualization of climate and remote sensing data for advanced natural resource monitoring and process understanding. *B. Am. Meteorol. Soc. 98*, 2397-2410.

IPBES, 2018. Summary for Policy Makers of the Thematic Assessment Report on Land Degradation and Restoration of the Intergovernmental Science-Policy Platform on Biodiversity and Ecosystem Services. R. Scholes, L. Montanarella, A. Brainich, N.Barger (Eds.), *Intergovernmental Science-*

570 *Policy Platform on Biodiversity and Ecosystem Services.* Bonn, Germany (2018)

571 Jewitt, D., Goodman, P.S., Erasmus, B.F.N., O'Connor, T.G., Witkowski, E.T.F., 2015. Systematic land-
572 cover change in KwaZulu-Natal, South Africa: Implications for biodiversity. SA J. Sci. 111(9-10):
573 Article No. 2015-0019.

574 Liu, H.Q., Huete, A., 1995. Feedback based modification of the NDVI to minimize canopy background
575 and atmospheric noise. *IEEE Trans. Geosci. Remote Sens.* 33(2), 457-465. DOI:
576 https://doi.org/10.1109/36.377946

577 Macharia, P.N., Ekaya, W.N., 2005. The impact of rangeland condition and trend to the grazing
578 resources of a semi-arid environment in Kenya. *J. Hum. Ecol.* 17, 143–147. DOI:
579 https://doi.org/10.1080/09709274.2005.11905769

580 Maestre, F.T., Eldridge, D.J., Soliveres, S., Kéfi, S., Delgado-Baquerizo, M., Bowker, M.A., García-
581 Palacios, P., Gaitán, J., Gallardo, A., Lázaro, R., 2016. Structure and functioning of dryland
582 ecosystems in a changing world. *Annu. Rev. Ecol. Evol. Syst.* 47, 215–237.

583 Mann, H.B., 1945. Nonparametric Tests Against Trend. *Econometrica*. 13, 245–259.
584 https://doi.org/10.2307/1907187

585 Masek, J.G., Vermote, E.F., Saleous, N.E., Wolfe, R., Hall, F.G., Huemmrich, K.F., Gao, F., Kutler, J., Lim,
586 T.-K., 2006. A Landsat surface reflectance dataset for North America, 1990-2000. *IEEE Geosci.*
587 *Remote Sens. Lett.* 3, 68–72. https://doi.org/10.1109/LGRS.2005.857030

588 Masubelele, M., Hoffman, M.T., Bond, W.J., 2015. Biome stability and long-term vegetation change in
589 the semi-arid, south-eastern interior of South Africa: a synthesis of repeat photo-monitoring
590 studies. *SA J. Bot.* 101: 139-147. https://doi.org/10.1016/j.sajb.2015.06.001

591 Melaas, E.K., Friedl, M.A., Zhu, Z., 2013. Detecting interannual variation in deciduous broadleaf forest
592 phenology using Landsat TM/ETM+ data. *Remote Sens. Environ.* 132, 176–185.
593 https://doi.org/10.1016/j.rse.2013.01.011

594 Mganga, K. Z., Musimba, N. K. R., & Nyariki, D. M., 2015. Combining sustainable land management
595 technologies to combat land degradation and improve rural livelihoods in semi-arid lands in
596 Kenya. *Environ. manage*. *56*(6), 1538-1548.

597 Mucina, L., Rutherford, M.C. and Powrie, L.W., 2018. The Vegetation Map of South Africa, Lesotho and
598 Swaziland. South African National Biodiversity, Cape Town.

599 Nkambule, P., Blignaut, J.N., Vundla, T., Morokong, T., Mudavanhu, S., 2017. The benefit and costs of

clearing invasive alien plants in northern Zululand, South Africa. *Ecosyst. Serv.* 27: 203-223. DOI: 10.1016/j.ecoser.2017.04.011

O'Connor T.G., Puttick, J.R., Hoffman, M.T., 2014. Bush encroachment in southern Africa: changes and causes. *Afr. J. Range For. Sci.* 31, 67-88. https://doi.org/10.2989/10220119.2014.939996

Pasquarella, V.J., Holden, C.E., Kaufman, L., Woodcock, C.E., 2016. From imagery to ecology: leveraging time series of all available Landsat observations to map and monitor ecosystem state and dynamics. *Remote Sens. Ecol. Conserv.* 2, 152–170. https://doi.org/10.1002/rse2.24

Pellegrini, A.F.A., Pringle, R.M., Govender, N., Hedin, L.O., 2017. Woody plant biomass and carbon exchange depend on elephant-fire interactions across a productivity gradient in African savanna. *J. Ecol.* 105, 111-121. DOI: 10.1111/1365-2745.12668

Pettorelli, N., Vik, J.O., Mysterud, A., Gaillard, J.-M., Tucker, C.J., Stenseth, N.C., 2005. Using the satellite-derived NDVI to assess ecological responses to environmental change. *Trends Ecol. Evol.* 20, 503–510. https://doi.org/10.1016/j.tree.2005.05.011

Pettorelli, N., Laurance, W. F., O'Brien, T. G., Wegmann, M., Nagendra, H., Turner, W., 2014. Satellite remote sensing for applied ecologists: opportunities and challenges. *J. Appl. Ecol*. 51, 839-848. doi:10.1111/1365-2664.12261

Reiche, J., Hamunyela, E., Verbesselt, J., Hoekman, D., Herold, M., 2018. Improving near-real time deforestation monitoring in tropical dry forests by combining dense Sentinel-1 time series with Landsat and ALOS-2 PALSAR-2. *Remote Sens. Environ*. *204*, 147-161.

Roy, D.P., Kovalskyy, V., Zhang, H.K., Vermote, E.F., Yan, L., Kumar, S.S., Egorov, A., 2016. Characterization of Landsat-7 to Landsat-8 reflective wavelength and normalized difference vegetation index continuity. *Remote Sens. Environ.* 185, 57–70. https://doi.org/10.1016/j.rse.2015.12.024

Sen, P.K., 1968. Estimates of the Regression Coefficient Based on Kendall's Tau. *J. Am. Stat. Assoc.* 63, 1379–1389. https://doi.org/10.1080/01621459.1968.10480934

Sinclair, A.R.E., Fryxell, J.M., 1985. The Sahel of Africa: ecology of a disaster. *Can. J. Zool.* 63, 987–994.

Shackleton, C.M., Mograbi, P.J., Drimie, S., Fay, D., Hebinck, P., Hoffman, M.T., Maciejewski, K., Twine, W., 2019. Deactivation of field cultivation in communal areas of South Africa: Patterns, drivers and socio-economic and ecological consequences. *Land Use Policy* 82: 686-699. DOI: 10.1016/j.landusepol.2019.01.009

630 Singh, J., Levick, R.S., Guderle, M., Scmullius, C., Trumbore, S.E., 2018. Variability in fire-induced
631 change to vegetation physiognomy and biomass in semi-arid savanna. *Ecosphere* 9, Article
632 e02514. DOI: 10.1002/ecs2.2514

633 Skowno, A.L., Thompson, M.W., Hiestermann, J., Ripley, B., West, A.G., Bond, W.J., 2017. Woodland
634 expansion in South African grassy biomes based on satellite observations (1990-2013): general
635 patterns and potential drivers. Glob. Chang. Biol. 23, 2358-2369.
636 https://doi.org/10.1111/gcb.13529

637 Staylor, F.W., 1990. Degradation rates of the AVHRR visible channel for the NOAA 6, 7, and 9
638 spacecraft. *J. Atmos. Ocean. Technol.* 7, 411–423.

639 Svoray, T., Perevolotsky, A., Atkinson, P.M., 2013. Ecological sustainability in rangelands: the
640 contribution of remote sensing. *Int. J. Remote Sens.* 34, 6216–6242.
641 https://doi.org/10.1080/01431161.2013.793867

642 Tanre, D., Holben, B.N., Kaufman, Y.J., 1992. Atmospheric correction algorithm for NOAA-AVHRR
643 products: theory and application. *IEEE Trans. Geosci. Remote Sens.* 30, 231–248.

644 Thompson, M., Vlok, J., Rouget, M., Hoffman, M. T., Balmford, A., Cowling, R. M., 2009. Mapping
645 grazing-induced degradation in a semi-arid environment: a rapid and cost effective approach for
646 assessment and monitoring. *Env. Manag. 43*(4), 585.

647 Tucker, C.J., 1979. Red and photographic infrared linear combinations for monitoring vegetation.
648 *Remote Sens. Environ.* 8, 127–150. https://doi.org/10.1016/0034-4257(79)90013-0

649 Tucker, C.J., Pinzon, J.E., Brown, M.E., Slayback, D.A., Pak, E.W., Mahoney, R., Vermote, E.F., El Saleous,
650 N., 2005. An extended AVHRR 8-km NDVI dataset compatible with MODIS and SPOT vegetation
651 NDVI data. *Int. J. Remote Sens.* 26, 4485–4498. https://doi.org/10.1080/01431160500168686

652 Turpie, J.K., O'Connor, T., Mills, A., Roberson, H., 2007. The ecological and economic consequences of
653 changing land use in the southern Drakensberg Grasslands, South Africa. SA J.Econ. Manage. Sci.
654 10, 423-441.

655 United Nations, 2014. System of Environmental-Economic Accounting 2012 – Experimental Ecosystem
656 Accounting. Sales No. E.13.XVII.13.

657 Venter, Z.S., Cramer, M.D., Hawkins, H.-J., 2018. Drivers of woody plant encroachment over Africa.
658 *Nat. Commun.* 9. https://doi.org/10.1038/s41467-018-04616-8

659 Verbesselt, J., Hyndman, R., Newnham, G., Culvenor, D., 2010. Detecting trend and seasonal changes

660 in satellite image time series. *Remote Sens. Environ.* 114, 106–115.
661 https://doi.org/https://doi.org/10.1016/j.rse.2009.08.014

662 Wessels, K.J., Prince, S.D., Malherbe, J., Small, J., Frost, P.E., VanZyl, D., 2007. Can human-induced land
663 degradation be distinguished from the effects of rainfall variability? A case study in South Africa.
664 *J. Arid Environ.* 68, 271–297.

665 Wessels, K.J., van den Bergh, F., Scholes, R.J., 2012. Limits to detectability of land degradation by trend
666 analysis of vegetation index data. *Remote Sens. Environ.* 125, 10-22. DOI:
667 10.1016/j.rse.2012.06.022

668 Wilcox, R.R., 2010. Fundamentals of modern statistical methods: Substantially improving power and
669 accuracy. Springer.

670 Witt, A., Kiambi, S., Beale, T., & Van Wilgen, B., 2017. A preliminary assessment of the extent and
671 potential impacts of alien plant invasions in the Serengeti-Mara ecosystem, East Africa. *Koedoe,*
672 59, 1-16.

673 Woodcock, C.E., Allen, R., Anderson, M., Belward, A., Bindschadler, R., Cohen, W., Gao, F., Goward,
674 S.N., Helder, D., Helmer, E., Nemani, R., Oreopoulos, L., Schott, J., Thenkabail, P.S., Vermote, E.F.,
675 Vogelmann, J., Wulder, M.A., Wynne, R., 2008. Free Access to Landsat Imagery. *Science*
676 *320*(5879), 1011 LP-1011. https://doi.org/10.1126/science.320.5879.1011a

677 Wulder, M.A., Masek, J.G., Cohen, W.B., Loveland, T.R., Woodcock, C.E., 2012. Opening the archive:
678 How free data has enabled the science and monitoring promise of Landsat. *Remote Sens.*
679 *Environ.* 122, 2–10. https://doi.org/10.1016/j.rse.2012.01.010

680 Xue, J., Su, B., 2017. Significant remote sensing vegetation indices: a review of developments and
681 applications. *J. Sensors* 2017.

682 Yang, Y., Erskine, P.D., Lechner, A.M., Mulligan, D., Zhang, S., Wang, Z., 2018. Detecting the dynamics
683 of vegetation disturbance and recovery in surface mining area via Landsat imagery and
684 LandTrendr algorithm. *J. Clean. Prod.* 178, 353–362.
685 https://doi.org/https://doi.org/10.1016/j.jclepro.2018.01.050

686 Zhu, Z., 2017. Change detection using landsat time series: A review of frequencies, preprocessing,
687 algorithms, and applications. *ISPRS J. Photogramm. Remote Sens.* 130, 370–384.
688 https://doi.org/10.1016/j.isprsjprs.2017.06.013

689 Zhu, Z., Piao, S., Myneni, R.B., Huang, M., Zeng, Z., Canadell, J.G., Ciais, P., Sitch, S., Friedlingstein, P.,
690 Arneth, A., Cao, C., Cheng, L., Kato, E., Koven, C., Li, Y., Lian, X., Liu, Y., Liu, R., Mao, J., Pan, Y.,

691 Peng, S., Peñuelas, J., Poulter, B., Pugh, T.A.M., Stocker, B.D., Viovy, N., Wang, X., Wang, Y., Xiao,
692 Z., Yang, H., Zaehle, S., Zeng, N., 2016. Greening of the Earth and its drivers. *Nat. Clim. Chang.* 6,
693 791.

694

695

696 Table 1. Description of greening and browning scenarios illustrated in Fig. 3 and 4. Repeat photographs
697 are licensed under Creative Commons licence CC-BY.

Trend	Biome	Figure reference	Coordinates	Scenario	Photo attribution
Greening	Grassland	3A	-30.526, 29.050	Bush encroachment by *Acacia mearnsii* and *Leucosidea sericea*	rePhotoSA image #45
	Grassland	3B	-28.873, 28.242	Increase of woody plant cover in erosion gullies - potential restoration signal	DigitalGlobe
	Nama-Karoo	3C	-32.331, 24.441	Increase in grass cover and vegetation vigor	rePhotoSA image #3
	Savanna	3D	-28.308, 24.779	Woody cover loss on slopes but increase in grass vigor on plains	DigitalGlobe
Browning	Savanna	4A	-26.502, 31.596	Clearing of woody plants for establishing residential buildings	DigitalGlobe
	Nama-Karoo	4B	-33.174, 23.430	Right-hand side of the fence line reflects decline in cover of the dominant shrub, *Portulacaria afra* (spekboom)	rePhotoSA image #35
	Fynbos	4D	-34.083, 18.402	Manual clearing of alien pine trees from the crest of the slope.	rePhotoSA image #52
	Succulent-Karoo	4C	-28.589, 20.156	Gradual loss of vegetation vigor with potential loss of perennial herbs	rePhotoSA image #35

698

699

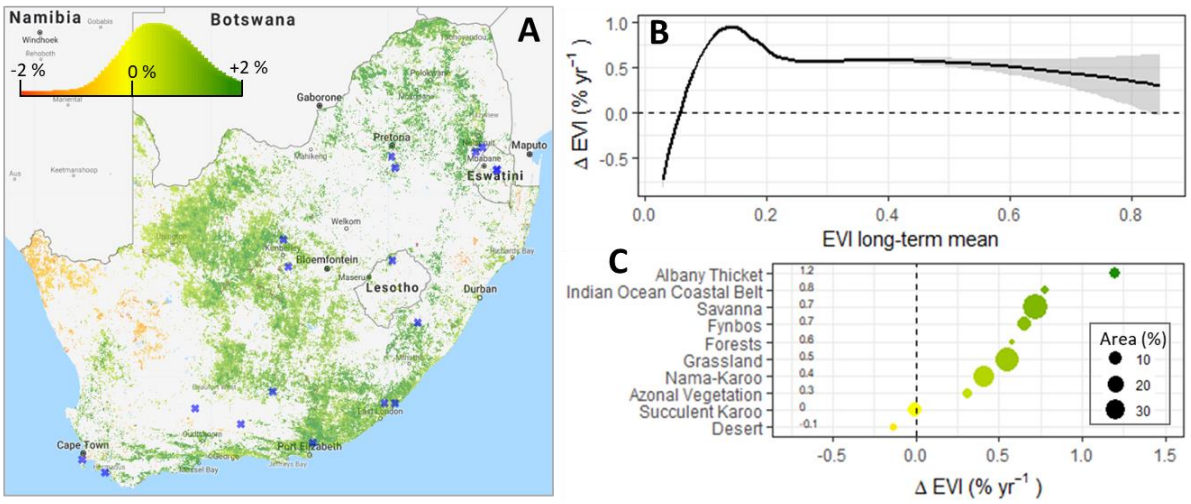

700

701 **Figure 1.** Average annual change in EVI between 1984 and 2018 (A). Change is expressed as a
702 percentage of the baseline (1984) EVI value and is derived from the slope and y-intercept of the
703 regression line through annual medoid composites of Landsat EVI. Non-significant trends are masked
704 (p>0.05) and points of local-scale validation are shown in blue. The colour scale depicts the distribution
705 of the data in A prior to significance masking. A loess regression line between the annual average
706 change and the long-term mean is plotted with a 95% confidence interval ribbon based on a 10 x 10
707 km aggregation grid (B). Mean annual EVI change values are presented for the major biomes in South
708 Africa after masking any non-natural land use (C). Data points are sized relative to the area covered
709 by the respective biome and mean values have been added to the left of the plot space.

710

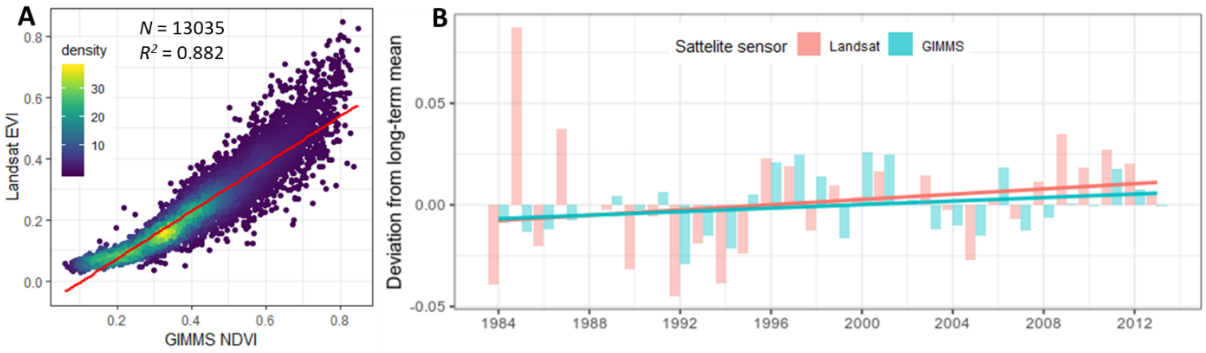

711

712 **Figure 2.** Comparison of mean EVI and NDVI values derived from Landsat and GIMMS sensors,
713 respectively, between 1984 and 2013 for all GIMMS pixels within South Africa (A). The density of data
714 points is indicated by the colour scale and the sample size (N) and R^2 value for the linear trend line
715 (red) are presented. The annual deviation from the long-term mean is plotted in B with a linear trend
716 line for each sensor.

717

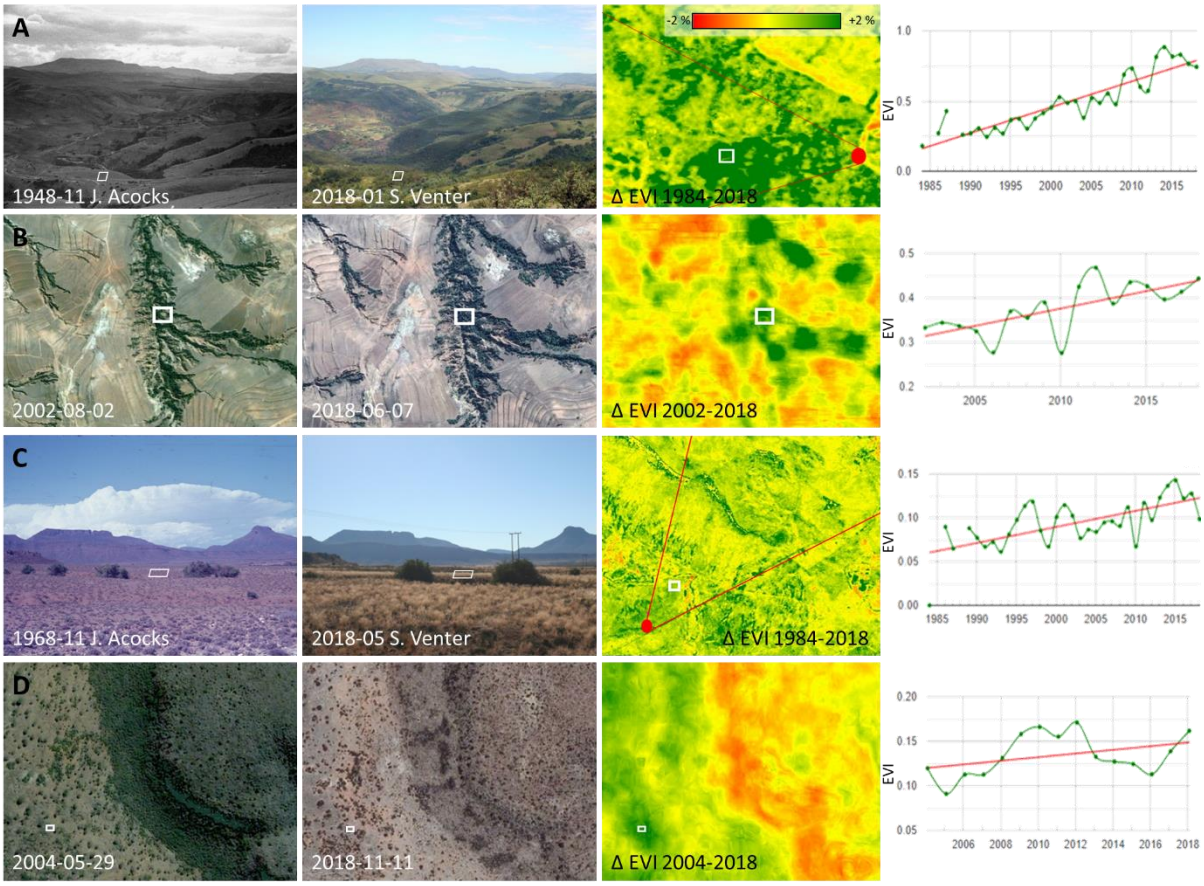

718

719 **Figure 3.** Landscape-scale EVI greening trends illustrated and interpreted with repeat ground (A, C)
720 and very-high resolution satellite (B, D) photographs. The photo location and approximate field of view
721 for ground photographs are shown in red in A and C. The average Landsat-derived annual change in
722 EVI are mapped for each pixel in the third column and is expressed as a percentage of the baseline EVI
723 value. Annual timeseries are plotted for the selected pixels (white squares) in the fourth column and
724 Sen's slope regression lines are plotted in red. See Table 1 for scenario descriptions.

725

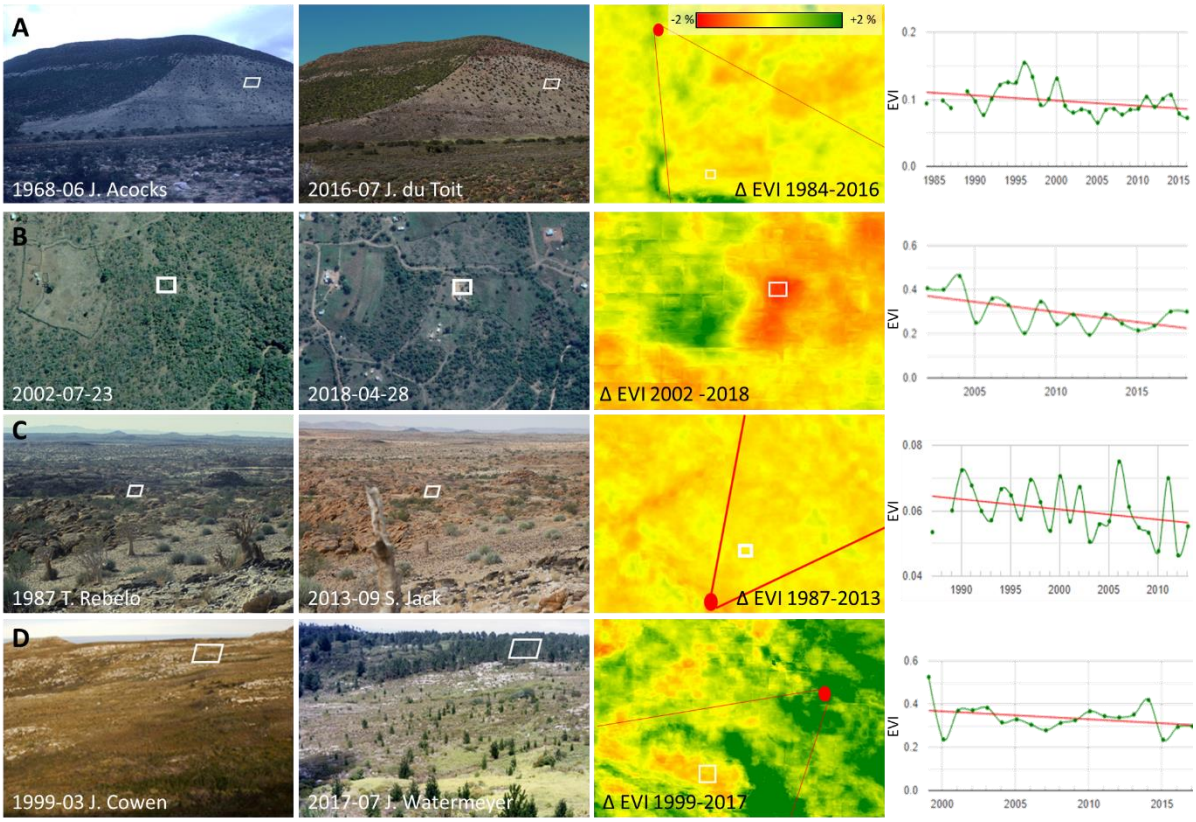

726

727 **Figure 4.** Landscape-scale EVI browning trends illustrated and interpreted with repeat ground (A, C,
728 D) and very-high resolution satellite (B) photographs. See Fig. 3 caption for further details on figure
729 layout and Table 1 for scenario descriptions.

730

Venter, Alexander Samuel; Scott, Samantha Luise; Desmet, Philip G.; Hoffmann, Michael Timm.
Application of Landsat-derived vegetation trends over South Africa: Potential for monitoring land degradation and restoration. Ecological Indicators 2020 ;Volum 113.
10.1016/j.ecolind.2020.106206 CC-BY-NC-ND

731

732